A Novel Cyclopropenyl Fatty Acid Library Reveals Tissue-Specific Preferences for Regulatory T Cell Uptake Through Click-Chemistry

Authors:

Graham Heieis[1,*,#], Luuk Reinalda[2,*], Laura I. Bogue[2], Kas Steuten[2], Connor Corrigan[3], Xinyuan Wang[3], Kristine Bertheussen[2], Marouane el Boujadayni[2], Jeroen M. Punt[5], Wouter P.F. Driever[5], Linda V. Sinclair[4], Mario van der Stelt[5], Bart Everts[1], David K. Finlay[3#],Sander I. van Kasteren[2,#]

Affiliations:

[1] Leiden University Medical Center for Infectious Disease, Albinusdreef 2, Leiden, The Netherlands,

[2] Department of Chemical Biology and Immunology, Leiden Institute of Chemistry, Einsteinweg 33, Leiden, The Netherlands

[3] School of Biochemistry and Immunology, Trinity Biomedical Sciences Institute, Trinity College Dublin, 152-160 Pearse Street, Dublin, Ireland

[4] 1Division of Cell Signalling and Immunology, School of Life Sciences, University of Dundee, Dundee, United Kingdom

[5] Department of Molecular Physiology, Leiden Institute of Chemistry, Einsteinweg 33, Leiden, The Netherlands

[*]Equal Contribution

[#]Correspondence: G.A.Heieis@lumc.nl, finlayd@tcd.ie, S.I.van.kasteren@chem.leidenuniv.nl

Abstract:

Immune function is critically dependent on the nutrient microenvironment, of which fatty acids are central. Tools are lacking to quantify fatty acid uptake at the single-cell level, which has hindered understanding how primary immune cells use them in physiological settings. Here we show the synthesis and utilization of novel cyclopropenyl-fatty acids (cpFA) of different saturation and chain length, that can be detected by click chemistry. We validated that CpFA are compatible with downstream omics pipelines and thus could be used to determine phenotypic links to relative uptake. Using cpFA, we found that $CD4^+$ regulatory T cells increase arachidonic acid uptake selectively in the intestine. RORγt$^+$ Tregs possessed superior Cp-arachidonic acid uptake in the mesenteric lymph node, compared to the small intestine, suggesting cell-intrinsic and niche factors control arachidonic acid uptake. CpFA are therefore a key technological advancement in immunometabolism that can reveal FA preferences of immune cells in tissues at the single cell level.

Conflicts:

The authors have no conflicts to declare.

Acknowledgements:

The authors would like to acknowledge the European Research Council for funding to SIvK (ERC CoG 865175 — KineTic) and DKV (ERC CoG 770769) MvdS and SIvK were co-recipient of the NWO-Gravitation Grant 'iCNS'.

Introduction

Metabolic adaptation is central to immune cell function. The metabolic state of an immune cell is shaped by its developmental stage, activation state and nutrient microenvironment.[1,2] Understanding nutrient uptake is therefore paramount for identifying metabolic bottlenecks in immune cells that underly their ability to function in distinct tissue niches.[3,4] Whereas core nutrients such as glutamine and glucose have well-characterized transporter systems allowing for easy manipulation of cellular uptake, fatty acid (FA) transport mechanisms are more promiscuous and complicated by their ability to both be transported, as well as passively insert in, and diffuse across membranes, sometimes aided by intracellular lipid shuttling proteins. The nature of FA transport therefore bars utilization of transgenic or pharmacological targeting methods. Workflows instead rely on supplementation of a particular FA in otherwise FA-free conditions and lipidomics. Both are hindered by the need for in vitro culture and isolation of bulk populations. Fluorophore-tagged lipids are an alternative for single-cell analysis, but structural differences may not accurately mimic native uptake kinetics, and sensitivity to fixation limits their use to live cell assays. Thus, new methods to study FA uptake are needed.

We aimed to overcome these drawbacks using bioorthogonal click chemistry.[5,6] This approach relies on synthesizing a nutrient mimic containing a non-naturally occurring chemical group that minimizes changes to the natural biochemical properties.[7] The modified group can then be detected by a "click" reaction that attaches a fluorescent label[8]. The use of click chemistry to quantify the rate of uptake of a given nutrient was recently described for glutamine, making it a powerful tool to study nutrient uptake rates in immunometabolism.[9] The use of clickable FAs containing an alkyne group has already been reported using cell lines[10–12], however, the copper-catalyzed Huisgen cycloaddition (CuAAC)-reaction required for alkyne-labelling is not live cell compatible, due to copper toxicity.

Recently, our group reported the use of sterculic acid, a natural oleic acid analog produced by plant species *Sterculia foetida*, as a method to determine oleic acid uptake.[13] Instead of an alkyne, sterculic acid (SA) possesses a cyclopropene (cp) group that can react spontaneously with electron-deficient dienes through the *inverse electron-demand Diels-Alder* reaction (IEDDA).[14–16] This reaction proceeds in absence of a toxic catalyst and is thus live cell compatible. Thus, using a fluorescently labelled cell-permeable reactive group, such as a BODIPY-tetrazine, allowed live quantification of sterculic acid (further referred to as cyclopropenyl oleic acid, cpOA).[13] We show that live cell-sorting of immune cells according to high or low cpOA uptake is compatible with downstream workflows such as flux analysis and proteomics. We alsoe report the chemical synthesis and biological validation of five additional cpFAs whose native analogs are abundantly found in circulation, namely the saturated FAs (SFA) palmitic acid (PA) and stearic acid (SA), the monounsaturated fatty acid (MUFA) palmitoleic acid (POA), and the polyunsaturated FAs (PUFA) linoleic acid (LA) and arachidonic acid (AA), allowing the comparison of uptake of different FA species across different immune cell types.

To further investigate how FA uptake is partitioned within the immune system, we asked whether T cells display distinct cpFA preference according to their tissue location. Our data reveals regulatory T cells (Tregs) dwelling in the intestinal lamina propria have a particular preference for AA. While peripherally-derived, RORγt^{+} Tregs took up most of the cp-labelled AA (cpAA) in the draining lymph node. This increased uptake was absent in the intestine, due to higher uptake by RORγt^{-} Tregs. Together, these data indicate both cell-intrinsic and environmental drivers of AA uptake in the intestine. Overall, we hereby demonstrate the ability of clickable cpFA in revealing novel metabolic characteristics of in vivo immune populations.

Results

Sterculic acid (cpOA) identifies distinct uptake patterns in ex vivo and in vitro-activated murine splenocytes

To confirm that cpFA can be used to measure uptake in primary immune cells we pulsed total murine splenocytes directly ex vivo with cpOA at an approximately physiological concentration (25µM).[22] Uptake was highly heterogenous between, and within, populations (**Figure 1A**). Dendritic cells (DCs) and monocytes displayed the highest cpOA uptake, followed by neutrophils. T and B lymphocytes showed comparably low uptake (**Figure 1B**). However, $CD4^+$ T cells expressing CD44, indicative of previous activation, possessed greater uptake than $CD44^{Lo}$ naïve T cells, consistent with the role of oleic acid in supporting effector responses (**Figure 1C**). We sought to confirm that cpOA uptake is increased during T cell activation by stimulating splenocytes with αCD3/αCD28, which preferentially activates and expands $CD4^+$ T cells. In accordance with the ex vivo difference, cpOA detection was significantly higher in $CD4^+$ T cells following stimulation, compared to those from unstimulated splenocytes (**Figure 1D**), and at 37 °C, compared to 4 °C; the latter temperature abolishing energy-dependent processes of uptake (**Figure 1D**). DCs can also be separated into separate subsets based on their role in primarily driving cytotoxic $CD8^+$ or helper $CD4^+$ T cell responses, known as cDC1 and cDC2 sub-types.[17] How FA uptake differs between these cells is unknown. We here found that cDC2 had higher uptake propensity than cDC1, suggesting a possible increased dependency of cDC2 on external FA (**Figure 1E**).

A key advantage of using cpFA is the fact that the compatible click reaction, the IEDDA, used to visualize FA-uptake is live cell compatible (**Figure S1**). The IEDDA relies on cell-permeable low-toxic fluorophores for the visualisation and does not require toxic catalysts. In addition, background reactivity is masked by the tetrazine reaction partner of the cp-group, as this chemical group is a potent quencher of fluorophores, resulting in increased signal-to-noise ratios due to fluorescence turn-on upon reaction with the cpFAs.[14] We next sorted tge $CD3^+CD4^+$ T cells from naïve or CD3/CD28 activated splenocytes according to low (bottom quartile) or high (top quartile) cpOA uptake (**Figure S2 for sorting strategy**). Back-gating to forward and side scatter for these cells showed that FA-high cells were larger and more granular (**Figure 2A**), both for naïve and activated T cells. After sorting, the live, sorted cells were used for extracellular flux analysis and proteomics. Flux analysis by Seahorse (**Figure 2B and Figure S3**), showed that the low uptake naïve cells were highly reliant on oxidative phosphorylation and less on glycolysis. High cpOA-uptake naïve T cells, on the other hand, showed an inverse metabolic profile (**Figure 2B**). Activated T cells did not show this distinction (**Figure 2B**).

To identify whether this difference in metabolism translated to any changes in protein expression, the high/low uptake fractions of the naïve and activated populations were also subjected to proteomic analysis. Interestingly, in naïve T cells only 22 proteins were upregulated in the cpOA-high population compared to the low, and one downregulated. This may be due to the overall low metabolic and translational activity in naïve cells (**Figure 2C, Table S1)**.[18] The difference between the activated high/low populations was more striking, with 154 proteins upregulated and 204 proteins downregulated in the cpOA-high population compared to the low (**Figure 2C, Table S2**). High uptake $CD4^+$ T cells largely showed increased expression of proteins strongly linked to activation, such as participating in positive regulation of cell cycle and mitosis, suggesting higher uptake corresponds with those cells that are activated earlier or more strongly (**Figure 2D**). Proteins involved in metabolic pathways that support T cell activation, including glycolysis[19], FA synthesis[20] and the mevalonate pathway[21], were also all upregulated in cpOA-high cells (**Figure S4**). These data illustrate the ability

and potential of combining cpFA uptake of live immune cells with omics- based analysis to further our understanding of how metabolic programming connects to function and phenotypes of immune cells.

Synthesis other cyclopropenyl fatty acids (cpFA)

Having established the use of a naturally occurring cpFA in linking uptake to immune phenotypes, we sought to expand our library of cpFA species. We therefore synthesized a selection of cpFA with different saturations, whose native counterparts are found at high concentrations in human blood[22]: saturated palmitic acid(PA) and stearic acid(SA), monounsaturated palmitoleic acid(PLA), and polyunsaturated arachidonic acid(AA) and linoleic acid(LA).

We postulated that for the SFAs palmitic acid and stearic acid an analogue bearing a terminal methyl cyclopropene with the same carbon chain length would serve as the best possible mimic of the natural SFAs PA and SA (**Figure 3A**, Compound **cpPA, cpSA**). The analogue of MUFA palmitoleic acid is based on naturally occurring oleic acid analogue **cpOA** where the double bond is replaced by a cyclopropene (**Figure 3A**, Compound **cpPLA**). In analogs of the ω-6 PUFAs linoleic acid **cpLA** and arachidonic acid **cpAA**, the double bond in the ω-6-position could be replaced by a cyclopropene, to keep the structural dissimilarity due to the different bond angle minimal.

Various routes towards the synthesis of sterculic acid have been reported, that can be applied to the synthesis of SFA and MUFA, but not PUFA analogues, of which the rhodium catalyzed [2+1] cycloaddition between a metal carbene formed from ethyl diazoacetate (EDA) and an alkyne has been most extensively investigated.[23] **cpPLA** could indeed be synthesized in 2.4% yield over 5 steps (**Figure S5**) by this method. The final step was, however, capricious and hard to get consistent. **cpPA, cpSA** and **cpOA** were therefore synthesized using tribromocyclopropane as a precursor for the lithiated cyclopropene nucleophile (**Figure 3B**) in 2.5 – 11.5% yield over 5 steps.

Synthesis of polyunsaturated **cpLA** and **cpAA** could not be achieved by this method. We therefore chose to pursue a Wittig olefination to connect the cyclopropene and unsaturated FA-parts of the molecule (**Figure 3C, D and S6**)[24]. It is important to note that introduction of the aldehyde and cyclopropene on the same synthon did not yield a stable product (**s7; Figure S6A,B**). The inverse approach, where the phosphonium bromide **15** was reacted with fatty ester aldehyde **16** did prove successful (**Figure 3C**). Alcohol **13** was synthesized by ring-opening of ethylene oxide, catalyzed by BF_3·OEt in presence of the lithiated cyclopropene nucleophile from **12**. We had previously found that 1,3-substituted cyclopropene β-alcohols were incompatible with the Appel(-like) reaction. Appel-like conditions using *N*-bromosuccinimide on our 1,2-substituted substrate, however, did afford stable cyclopropene bromide **14** in 59% yield. An overnight substitution reaction with triphenylphosphine under reflux conditions in acetonitrile yielded the target cyclopropene phosphonium bromide **15** in 23% yield over 3 steps. Aldehyde **16** was synthesized in five steps from nonane-1,9-diol in 37% yield (**Figure S7**). The phosphorus ylide of **15** was formed *in situ* using NaHMDS and reacted with aldehyde **16** to yield the cyclopropene linoleic methyl ester **17**. Subsequent saponification yielded **cpLA (Figure 3C**), to the best of our knowledge the first example of the synthesis of a cyclopropene-containing PUFA analogue.

We next attempted the synthesis of cpAA using a Wittig-based sequence, but due to poor stereoselectivity of the Wittig reactions and troublesome acetal deprotection we instead used the bis-alkyne **s15** as key intermediate to synthesize the aldehyde **18** (**Figure S8**).[25] Aldehyde **18** was synthesized from 5-hexynoic acid in 5 steps in 3% yield, preparative HPLC purification was necessary to ensure the exclusive presence of the alkene following the selective reduction. Finally, a Wittig

reaction between aldehyde **18** and phosphonium bromide **15** yielded cyclopropene arachidonyl methyl ester **19** that could be saponified to yield **cpAA** (**Figure 3D**). In conclusion, five cyclopropenyl analogues of saturated, mono-unsaturated and polyunsaturated FAs were synthesized. The latter being the first reported examples of such syntheses.

Validation of novel cpFA

All cpFA showed detectable uptake in primary splenocytes, compared to cold controls and background (**Figure 4A**). Importantly, competing the cpFA with titrating concentrations of the corresponding native FA show a concentration dependent reduction in cpFA uptake (**Figure 4B**). Similar to cpOA, monocytes and DCs consistently exhibited the highest uptake, followed by neutrophils and subsequently lymphocytes (**Figure 4C**). $CD4^{+}CD44^{Hi}$ effector/memory T cells also ubiquitously showed increased uptake over naïve $CD44^{Lo}$ (**Figure 4D**). When looking at DC subsets we noticed that the MUFA cpPLA, showed higher uptake in DC2 compared to DC1 analogous to cpOA (**Figure 4E, Figure 1E**). This was observed to a lesser extent for the PUFAs and not at all for the SFAs, which may point towards a specific preference of MUFAs in DC2 compared to DC1.

Metabolic competition in nutrient microenvironments is a key determinant of immune function. To determine if cpFA could be used to visualize nutrient competition in a mixed cellular milieu, we looked at how increasing concentrations (0.1-500 µM) of cpFA affected the relative uptake by different splenic populations (**Figure 4F**). All populations showed increased cpFA uptake with increasing concentration. However, the rate of increase was different for different splenic sub-population. The change in uptake between 10 µM and 50 µM was particularly big, indicating that nutrient competition is important below 50 µM, the physiological concentration of these FAs.[22] DC, monocytes and neutrophils, which already showed the highest FA-uptake capacity, also exhibited the steepest increases in uptake with increasing cpFA concentrations (**Figure 4F**), and leukocytes display lower changes in the rate of uptake. This suggests that these cells (which make up ~5% of total immune cells in the spleen) are outcompeted for FAs at lower concentrations by the high density of T and B cells. Higher FA concentrations thus allows them to increase their uptake as leukocyte uptake does not have this extra 'uptake bandwidth', which is highlighted by the lower rates of increase of both CD4 and CD8 T cell populations.

As an additional proof-of-concept, we evaluated how CD4 T cell uptake was affected by mixing total splenocytes with peritoneal exudate cells (PEC) that contain a high frequency of $CD11b^{+}$ myeloid cells (macrophages) that consume high amounts of FA (**Figure 4G**). $CD4^{+}$ T cells from the PEC already trended towards reduced uptake relative to the splenic population. Accordingly, mixing spleen and PEC cells significantly reduced uptake of spleen $CD4^{+}$ T cells, whereas those from the PEC were unaffected (**Figure 4H**). This further confirms that immune cells compete for cpFA at physiological concentrations of cpFA.

cpFA uptake by CD4+ Tregs is location and lineage dependent

Regulatory T cells (Tregs) are indispensable for immune regulation and, *in vitro*, have an increased dependency on FA oxidation compared to naïve or T effector (Teff) cells.[19] However, whether Tregs depend on specific FA for their metabolism or function has not been investigated, particularly *in vivo,* although it has recently been reported that oleic acid is important for the induction of thymic Tregs.[26] We profiled cpFA uptake by tissue $CD4^{+}$ T cells, including Tregs, *ex vivo* using one each of a SFA (cpPA), MUFA (cpOA) and PUFA (cpAA). A barcoding and pooling approach was used, followed by total CD3 T cell enrichment, to eliminate confounding effects of cell composition (**Figure 5A**). Total $CD4^{+}$ T cells

from the small intestine lamina propria (SILP) appeared to have enhanced uptake for all cpFA compared to the draining mesenteric lymph node (MLN), lung or spleen (**Figure 5B**). This was largely driven by an increased frequency of $CD44^{Hi}$ memory/effector cells that have higher uptake propensity (**Figure 5C**). When subsetting on different populations, $CD44^{Lo}$ naïve cells showed more comparable uptake across sites, although with a small but significant reduction in the spleen compared to all tissues, irrespective of the cpFA used (**Figure 5D-F**). $CD44^{Hi}$ Teff/mem uptake was similarly low in the spleen. Tregs, in contrast, showed a unique increase of cpAA uptake in the SILP compared to all other tissues (**Figure 5F**). Tregs from the SILP similarly had increased cpPA uptake compared to the spleen and MLN, but showed similar cpPA uptake as those found in the lung, indicating a possible shift toward PA acquisition in peripheral tissues (**Figure 5D**). Conversely, uptake of cpOA by Tregs remained consistent with those from lymphoid tissues and the lung (**Figure 5E**). To a lesser degree, cpAA uptake was also particularly higher in $CD44^{Hi}$ $CD4^{+}$ T cells from the SILP compared to other tissues (**Figure 5F**). However, when comparing across populations within a given tissue, intestinal Tregs still were found to have significantly greater uptake than $CD44^{Hi}$ Teff/mem, which was not the case for other tissues (**Figure 5F**). An increased preference for cpAA over cpOA by Tregs was also observed during in vitro differentiation (**Figure 5G**). Tregs polarized in vitro continued to increase their cpAA uptake at later stages post-activation, with significantly higher detection at 72h compared to 24h, whereas cpOA acid uptake was close to maximal at 24h. In vitro activated Teff, however, showed a continual increase in both cpAA and cpOA (**Figure 5G**). Thus these data provide evidence of a particular need for AA in induced Tregs.

The specifically high cpAA uptake for both $CD44^{Hi}$ and Tregs in the SILP might suggest that environmental factors in the intestine are responsible. However, it is also known that the intestine is enriched in peripherally derived $ROR\gamma t^{+}$ Tregs (**Figure 6A**), as well as $ROR\gamma t^{+}$ Th17/22 cells, that maintain immune tolerance and barrier function in response to the microbiota.[27,28] However, we found that this did not fully explain the difference in cpAA uptake, as no difference was found between $ROR\gamma t^{+}$ and $ROR\gamma t^{-}$ Tregs from the SILP (**Figure 6B**). However, in the intestinal draining MLN, $ROR\gamma t^{+}$ cells did show a significant increase in cpAA uptake compared to $ROR\gamma t^{-}$, so they were comparable to the intestinal Tregs (**Figure 6B,C**). This was true after further accounting for differences in activation status based on CD44 expression (**Figure 6D**). A similar observation was made for the Teff/mem population in the MLN, but to a smaller extent than Tregs. This trend for higher uptake in $ROR\gamma t^{+}$ Teff/mem was similarly seen in all tissues except the SILP (**Figure 6D**). Altogether, our data argue for both cell-intrinsic and environmental drivers of cpAA in Tregs found in the SILP. Furthermore, we have exemplified how our novel cpFA library can be used to reveal new aspects of immune cell metabolism in *ex vivo* settings.

Discussion

FAs have diverse roles in the immune system; however, the exact contribution and uptake of individual species has thus far been difficult to resolve. Here we report the synthesis and application of a chemically modified FA library that is used to measure cellular uptake of individual FAs via click chemistry. Incorporating a cycloproprene group into the carbon chains overcomes several limitations in existing methods that measure FA uptake. The current standard to determine nutrient uptake is using fluorescently tagged lipids. Yet, these modifications significantly alter the (bio-)chemical properties of the parent metabolite such that it alters transport specificity, as has recently been shown for the glucose analog 2NBDG.[29]

The exact mechanisms that allow FA transport across the plasma membrane remains poorly understood, but is thought to rely on a combination of passive insertion[30], and protein mediated assistance.[31] The attachment of a fluorescent (often BODIPY) group to the terminus to the headgroup

or the carbon tail of FAs significantly alters the polarity, hydrophobicity, size, and shape of the molecule compared to the parent FA. This consequently affects solubility, albumin binding, and the rate of membrane insertion, extraction and subcellular mobility.[32] A second caveat, is that BODIPY dyes can be sensitive to fixation which limits experiments to live acquisition. Conversely, alkyne-modified FA have also been extensively employed to study uptake[33], although never in primary immune cell populations. These, however, can only be labeled via the CuAAC-reaction[34], which requires a toxic copper-catalyst to catalyze the reaction, complicating the possibility of live-cell analysis[35]. Thus, our cpFA library has the advantage being both live and fixed cell compatible while closely maintaining native properties – the introduction of the clickable group only alters the molecule by one carbon atom – that we show by both sorting on high vs low uptake cells for subsequent sequencing and proteomics, as well staining for intranuclear Foxp3 to distinguish uptake in Tregs.

We used our new library of cpFA to interrogate how uptake of different FA species varied across immune subsets, with a focus on T cells. Our observations suggest both previously activated CD4 T cells and Tregs from murine tissues increase FA uptake over naïve cells, but that Tregs tend to have the highest uptake in line with previous studies. The seminal study by Mikalek *et al*.[19] showed that Tregs preferentially fuel beta-oxidation compared to activated $CD4^+$ effector subsets that rely on glucose. However, FA uptake in activated T cells is also substantially increased shortly after stimulation and required for their proliferation and effector function. A key regulatory component of immune responses that is also gaining appreciation is metabolic competition.[36–39] We demonstrate here that, in vitro, immune cells compete for cpFA at physiological concentrations. Thus, cpFA are a new tool that will be able to shed light on how FAs are partitioned within the immune system, and will be of particular interest in the context of immune activation when FA demand is rapidly increased. For instance, evidence suggests that interacting DC and T cells compete for glucose to control T cell priming[36]. Whether a similar phenomenon happens for FAs is a point of further investigation.

Evidence is also accumulating that not all FA are equal in the eyes of immune cells. During T cell activation only certain FAs, such as oleic acid, were able to restore proliferation compared to FA-free conditions[40]. Interestingly, saturation or carbon length alone did not appear to be the determining factor for these observations. Functions other than proliferation also have particular FA requirements. Linoleic acid was found to have no effect on T cell proliferation, but in CD8 T cells promotes mitochondrial fitness to enforce a memory-like phenotype, allowing superior anti-tumor activity.[41] A major caveat of this study, though, is the phenomenon was only described in vitro, and whether linoleic acid uptake is restricted in tumor-infiltrating T cells, or can be sustained by linoleic acid conditioned CAR-T cells, was not questioned. Thus, the cpFA we have developed will be important in supporting such studies by confirming uptake capacity ex vivo, and even in vivo.

Our data further indicate specific FA preferences in T cells, and show that Tregs from the intestine have a cell-intrinsic preference for cpAA, compared to the draining lymph, spleen or lung. We have previously found that macrophage metabolism is unique according to the resident tissue[1], while others have shown that changing the tissue environment leads to rapid metabolic adaptation.[42] Evidence suggests similar adaption for the formation of tissue resident T cells in response to infection.[43,44] How FA uptake differs across tissues at steady-state, however, has yet to be reported, which may have particular relevance for Tregs that are constantly guarding against unwanted immune activation. However, the finding that tissue resident memory T cells express distinct FA binding proteins depending on their tissue site may support tissue-specific preferences for certain FA.[43] A recent report has similarly suggested that in the intestine, Tregs preferentially use AA for the anabolic generation of membrane lipids, compared to conventional T cells.[45] This aligns with our data, in which we further argue that Tregs also selectively increase AA acid uptake. However, the functional significance of this remains to be elucidated.

The mechanisms of FA uptake remain controversial and largely undefined. In cell-free systems, FA can passively cross plasma membranes at similar rates irrespective of chain length or saturation.[30,31] However, the current consensus is that protein mediated transport is required in order to regulate FA uptake. The scavenger receptor CD36 is the main identified transmembrane transporter, and multiple FA transporters and binding proteins (FATPs and FABPs) have suspected roles in trapping/removing FA once they have reached the inner membrane. Little is known about FATP in immune cells, however CD36 may be expressed more highly in Tregs than Teff.[46,47] In general, it seems CD36 is upregulated by Tregs specifically in lipid-rich environments which may explain our findings.[45,48] How this selectively leads to AA uptake, however, remains an open question. It has been shown that immune cells have varied membrane compositions in blood.[49] leading to one hypothesis that membrane composition in Tregs is more permissive to AA transport. A second is that Tregs in the intestine express a set of FATP/FABP with high affinities for PUFA compared to Teff or other tissues. However, the complexity and unknowns of FA transport highlight the need for new tools, such as the ones we have developed here, to be able determine uptake of different species.

A final but important aspect to address is the great need for more specific and accurate methods to examine FA uptake in biological contexts. Fluorescently labeled FAs and quantum dot–conjugated FAs are some the most commonly used approaches for assessing single-cell FA uptake. However, it's important to note that these probes are not structurally similar to the native FAs they are meant to mimic. As a result, it's reasonable to suggest that they may not accurately reflect active FA transport, but instead measure the accumulation of the fluorescent probe within the cell. Additionally, many of these dyes lack lipid specificity, leading to non-specific uptake, and they are unable to distinguish between different FAs—which is a significant limitation given the distinct roles various FAs play in different cell types. Ultimately, these methods provide only a general indication of natural FA uptake mechanisms, rather than precise or specific insights.

Our novel cpFA analogs address the limitations of current FA tracing techniques by using cpFA specific molecules, that are structurally highly similar to the native FA moiety. Importantly, the fluorescent molecule is introduced only after the FA has completed uptake in the cell, enabling a more accurate mimic of natural FA uptake at the live, single-cell level. This approach offers improved specificity and fidelity in tracing FA dynamics compared to existing techniques. To add we have demonstrated how these novel cpFAs can be used in conjunction with many other standard techniques, adding to their applicability. Our approach opens up significant opportunities not only in the investigation of the FA requirements and transport in immune cell, but a wide range of applications and studies across different biological systems. Enabling a more accurate and specific tracing of FA uptake at a single-cell level, our cpFA analogs can facilitate a greater understanding of lipid metabolism and the role of different FAs in diverse physiological and pathological contexts.

Altogether, we here provide a novel set of specific FA analogs that can be applied in flexible settings to measure FA uptake. Our data demonstrate the power of click-chemistry based approaches to studying nutrient uptake within the highly dynamic immune system. We believe these tools will rapidly open doors to deepen our understanding of how unique FA molecules contribute to immune cells function in vivo.

Methods

Splenocyte isolation, stimulation and culturing.

Spleens were harvested from naïve C57BL/6 mice. To obtain a single-cell suspension of splenocytes, the spleens were minced with the flat end of a syringe plunger over a 70 µm cell strainer. The strainer was washed with single-cell suspension buffer (SCSB, 2% FCS and 1 mM EDTA in PBS), and the process was repeated until no more red tissue was visible in the strainer. The cells were pelleted at 300 *rcf* and 4°C for 10 min, the supernatant was discarded, and the cells were resuspended in 2 mL ACK lysis buffer (Thermo Fisher Scientific) per spleen, to remove red blood cells. After 5 min in the lysis buffer, cold PBS was added until 40 mL and the cells were pelleted at 500 *rcf* and 4°C for 5 min. The supernatant was discarded, and the cells were resuspended in SCSB and passed over a 40 µm cell strainer. The cells were pelleted at 300 *rcf* and 4°C for 10 min, the supernatant was discarded and the cells were resuspended in splenocyte medium (RPMI 1640 culture medium (Capricorn Scientific, #RPMI-HXA) supplemented with 10% FCS, GlutaMAX (2 mM), penicillin (100 I.U./mL), streptomycin (50 µg/mL), and 2-mercaptoethanol (50 µM)). The cells were counted using a haemocytometer before seeding. For experiments using solely unstimulated splenocytes, the cells were seeded directly for the respective experiments (see below).

For experiments using both stimulated and unstimulated splenocytes, half the wells of a Nunc™-treated 6-well plate (Thermo Fisher Scientific) were coated with Ultra-LEAF purified anti-mouse CD3ε antibody (BioLegend, 5 µg/mL) in sterile PBS for 2 h at 37°C. After 2 h the antibody was removed, and $15x10^6$ cells were seeded per well in 5 mL complete splenocyte medium supplemented with Ultra-LEAF purified anti-mouse CD28 antibody (BioLegend, 3 µg/mL) and recombinant murine IL2 (PeproTech, 10 U/mL). For unstimulated control cells, $15x10^6$ cells were seeded per well in 5 mL complete splenocyte medium supplemented with recombinant murine IL2 (PeproTech, 10 U/mL). All cells were incubated at 37°C, 5% CO_2 overnight. The next day, the activated and naïve cells were scraped, combined in separate tubes and centrifuged at 300 *rcf* for 10 min. The cells were resuspended in fresh splenocyte medium before being counted using a haemocytometer and seeded for experiments (see below).

Isolation of immune cells from tissues

Spleens or MLN were isolated from naïve C57BL/6 mice bred under specific pathogen free (SPF) conditions. To obtain a single cell suspension, spleens were minced with scissors in a 2 mL Eppendorf and shaken at 37 °C, 200 rpm for 30 minutes in 1 mg/mL of Collagenase IV reconstituted in RPMI medium. Tissue digestion was stopped by adding 1 mL of cold PBS containing 0.5% BSA and 2 mM EDTA (FACS buffer) and placed on ice. The remaining homogenate was crushed and washed through a 40 µM strainer into a 50 mL tube, spun at 400g for 5 minutes and resuspended in 3 mL of ACK lysis buffer to remove red blood cells. After 5 minutes in lysis solution, 7 mL of cold PBS was added and cells were spun, washed through a second 40 µM strainer and counted for plating using a hemocytometer.

Lung immune cells were isolated by mincing tissue in an Eppendorf tube and digesting in 1ml of 1mg/ml collagenase IV and 10U/ml DNAse in RPMI for 30 minutes at 37 in a shaking incubator at 180rpm. Digested tissues were washed through 40uM strainer in FACS buffer, spun down, and incubated for 5min in ACK lysis buffer to remove red blood cells, before spinning and resuspending in FACS buffer. To obtain immune cells from the small intestine the fat was first removed before cutting it open longitudinally on a PBS-soaked paper towel to gently scraping off feces and mucus. The intestine was then rinsed by shaking vigorously in a 50ml tube containing 20ml of Ca/Mg-free HBSS with 2mM EDTA (wash buffer), cut into 1-2 cm pieces and stored in wash buffer. The intestines then

underwent 3 rounds of washing to remove epithelial cells by shaking vigorously in wash buffer and incubating in a 37 shaking incubator at 180 rpm for 15 min. After the 3rd wash, intestines were rinsed once with RPMI and digested for 20 minutes in 10ml RPMI containing 1mg/ml Collagenase Type VIII and 10U/ml DNAse. Digested intestines were immediately topped up with 40ml RPMI with 10% serum, filtered through a 100uM strainer, and spun down. Cells were then resuspended in 30ml FACS buffer, filtered through a 40uM strainer, spun and resuspended in FACS buffer.

To obtain T cells from tissues, isolated immune cells were stained with a different fluorophore-labelled anti-CD45 antibody for 15 minutes at RT. Cells were then pooled per mouse in order to equalize the frequency of T cells: 5e6 lung cells, 5-10e6 SILP cells, 1e6 spleen and MLN cells. Total CD3+ cells were then isolated using magnetic negative selection

Preparation of fatty acid stocks

Solid cpFA stocks were first constituted in DMSO to make a 50 mM solution. Two 10x Step-wise dilutions were then done in RPMI medium containing 0.5% fatty acid free BSA to make a 5 mM and subsequent 0.5mM working stock. The 0.5 mM stock was then diluted to the appropriate 1x concentration to be added to isolated splenocytes.

Uptake assay

Working FA stocks were first pre-warmed in a 37 °C water bath. 1-2 x 10^6 splenocytes were plated in a 96-well V-bottom plate and kept on ice. Plated cells were washed twice in 200 µL of cold PBS. After washing, 100 µL of pre-diluted FA stocks (in the appropriate ratio with native FA for the competition experiment) were added directly to the splenocytes, which were immediately re-suspended by gentle pipetting. Resuspended cells were either placed in a 37 °C 5% CO_2 incubator or left on ice for 30 minutes, followed by addition of 100 µL cold PBS (0.5% BSA, 2mM EDTA) and spun at 400g for 5 minutes. Cells were washed an additional 2 times with cold PBS and left on ice for cell staining.

Cell staining and click-reaction for flow cytometry

Following FA uptake, cells were stained in 50 µl of Zombie NIR viability dye diluted 500x and antibodies that require live staining (anti-XCR1, anti-CD62L), in PBS for 15 minutes at room temperature. Cells were then washed 2x with 150 µL of cold PBS (0.5% BSA, 2mM EDTA), fixed with either 2% methanol-free formaldehyde for 10 minutes or Foxp3 fixation buffer for 30 minutes at room temperature, and washed twice with PBS. Cells were subsequently permeabilized by incubation in 50 µL of PBS containing 0.1% saponin and 1% BSA for 15 minutes, or washed in 1x Foxp3 permeabilization buffer. Permeabilized cells were washed with PBS, or perm buffer, and the tetrazine-cyclopropene click reaction was performed by diluting the indicated tetrazine-fluorophore in PBS and incubating in 50 µL at room temperature for 1 hour in the dark. Cells were washed 2 times in PBS and either left in the fridge until staining could be performed or immediately stained with 50 µL of antibody cocktail for the remaining surface markers for 30 minutes, washed twice with PBS, and resuspended in 150 µL PBS for acquisition. A full list of antibodies used can be found in Supplementary Table 1. Fully stained samples were acquired on a Cytek 5-laser Aurora and unmixed using SpectroFlo v3. Analysis was done using FlowJo v10, GraphPad Prism and OMIQ.ai.

Cell sorting for proteomics and Seahorse analysis.

Activated or naïve splenocytes were seeded evenly over the wells of three Nunc™-treated 6-well plates (Thermo Fisher Scientific) in 2 mL fresh splenocyte medium per well. To each well, 2 mL sterculic acid (200 µM) in splenocyte medium was added, to give a final sterculic acid-concentration of 100 µM. The cells were incubated at 37°C, 5% CO_2 for 15 min, to allow for uptake of the fatty acid. All wells were harvested, combined in 50 mL tubes, and washed with fresh medium (x1) and PBS (x1). Each

washing step consisted of spinning down (300 *rcf*, 5 min), aspirating supernatant, and resuspending in wash solution. After the last wash, the cells were resuspended in PBS supplemented with fluorophore **7** (1 µM) and incubated on ice for 35 min, to allow the fluorophore to react with sterculic acid. The cells were washed with cold PBS (x2), where each washing step consisted of spinning down (300 *rcf*, 5 min, 4°C), aspirating supernatant, and resuspending in wash solution. To perform a viability staining, the cells were resuspended in 750 µL of HBSS (Gibco, #14025092) supplemented with Zombie NIR (BioLegend, #423105, 1:500) and DNase I (Thermo Fisher Scientific, #90083, 30 U/mL), and incubated at RT for 15 min. The rest of the antibody cocktail was diluted in 250 µL HBSS and added to the cells to give a final volume of 1 mL. The following antibodies and dilutions (calculated with 1 mL final volume) were used: PE/Dazzle 594 anti-mouse CD3 (1:800), APC anti-mouse CD4 (1:400), eFluor450 anti-mouse CD44 (1:200), and PE-Cyanine7 anti-mouse CD62L (1:1000). The cells were incubated at RT for an additional 25 min, before addition of 10 mL FACS buffer (PBS with 0.2% BSA and 2 mM EDTA) and centrifugation at 300 *rcf*, 5 min. The cells were then washed with FACS buffer (x2), before being resuspended in ~1.5 mL FACS buffer. The samples were transported on ice and sorted using a BD FACS Aria III 4L (BD Biosciences, San Jose, CA, USA), following the gating strategy shown in **Figure S1A**. The experiment was repeated minimum as biological triplicates.

Seahorse analysis**.**

1-2x10^6 sorted low- and high-uptake cells were used to perform the Seahorse Real-Time ATP Rate Assay. Inhibitors and uncouplers were prepared in XF assay media, supplemented with 5 mM D-(+)-glucose for sequential addition at the appropriate final concentrations of oligomycin A (1.8 µM), and antimycin A (2 µM) (all Sigma-Aldrich). Cells were placed in a non-CO2 incubator at 37°C for 1 h prior to the assay. Basal respiration (OCR) and extracellular acidification rate (ECAR) were measured by the Seahorse Biosciences XFe24 Extracellular Flux Analyser (Agilent Technologies, Santa Clara, CA, USA). Oxygen consumption rates (OCR) and ECAR were measured and analysed using the Agilent online analysis tool. Values recorded were normalised to cell numbers seeded. Baseline readings were established, and the effects of specific inhibitors and uncouplers on OCR and ECAR were assessed using repeated measures ANOVA and plotted as bar charts, and scatter plots. Error bars indicating standard deviation were included to illustrate variability within the data.

Preparation of sorted samples for proteomics.

From the sorted cells (described above), 2x10^5 cells of each population were taken for total-digest proteomics. The samples were spun down at 300 *rcf*, 5 min, 4°C, and the supernatant was aspirated. The cell pellets were plunge frozen and stored at -80°C until further processing. Upon thawing of the samples, they were resuspended in 15 µL lysis buffer (250 mM sucrose, 5 mM EDTA, 1x cOmplete™ protease inhibitor (Roche) in PBS). The samples were lysed by sonication (Qsonica Q700 Microplate Sonicator, 4x10 s pulses, 10% amplitude, 0°C). Protein concentration was measured by Qubit Protein assay (Invitrogen) according to the manufacturer's protocol, and all samples were found to contain ~4 µg of protein. The proteins were precipitated by adding 500 µL cold (-80°C) acetone, vortexing, and incubating the samples at -80°C for 1 h. The samples were spun down at 20 000 *rcf*, 15 min, 4°C, and the supernatant was poured off. To wash, 300 µL acetone was added to each sample, followed by vortexing and sonication (2x10 s pulses, 10% amplitude, 0°C). The samples were incubated at -80°C overnight, before being spun down at 20 000 *rcf*, 15 min, 4°C. The supernatant was poured off, and the samples were airdried for 2 min to ensure all the acetone had evaporated. To redissolve and denature the proteins, 20 µL urea (8 M) in NH_4HCO_3 (100 mM), pH 8 was added, and the samples were shaken for 30 min at 37°C, 1000 rpm. The proteins were then reduced by addition of dithiothreitol (DTT, 5 mM) and the samples were shaken for 15 min at 65°C, 800 rpm. The samples were cooled down before addition of iodoacetamide (IAA, 10 mM) and incubation for 30 min at RT in the dark, to

acetylate all proteins. Unreacted IAA was quenched by addition of DTT (7 mM). All samples were diluted with 170 µL $CaCl_2$ (1 mM) in NH_4HCO_3 (20 mM) to ensure urea concentrations <1 M. All samples were transferred to Protein LoBind tubes (Eppendorf), and sequencing-grade trypsin (Promega, 0.2 µg) was added. The trypsin digestion mixture was shaken at 37°C, 1000 rpm overnight, before being quenched by addition of 5 µL 50% trifluoroacetic acid (TFA) in MilliQ. Peptides were desalted using Empore™ C18 StageTips (CDS Analytical) preconditioned with 50 µL MeOH, 50 µL of 0.05% (v/v) TFA in 60% (v/v) acetonitrile/MilliQ (solution B) and 50 µL 0.05% (v/v) TFA in MilliQ (solution A) by centrifugation (600 *rcf*, 2 min). The peptides were washed with solution A (100 µL, 800 *rcf*, 3 min) and eluted into new Protein LoBind tubes using solution B (100 µL, 800 *rcf*, 3 min). The samples were concentrated using an Eppendorf SpeedVac (Eppendorf Concentrator Plus 5301 or 5305) and stored at -80°C until measurement. Upon measurement, desalted peptide samples were reconstituted in 40 µL LC-MS solution (97:3:0.05 MilliQ, acetonitrile, TFA).

LC-MS/MS measurements.

Peptides (prepared as described above) were separated via nanoflow reversed-phase liquid chromatography using a nanoElute 2 LC system (Bruker Daltonics) coupled to a timsTOF HT mass spectrometer (Bruker) with 0.1% FA (solution A) and 0.1% FA/99.9% ACN (solution B) as the mobile phases. The samples were loaded on a trap column (PepMap C18, 5 mm x 0.3 mm, 5 µm, 100 Å, Thermo Scientific) followed by elution and separation on the analytical column (PepSep C18, 25 cm x 75 µm, 1.5 µm, 100 Å, Bruker) kept at 50 °C using a gradient of 2 - 25% solvent B in 25 min, 25 - 32% B in 5 min, 32 - 95% B in 5 min and 95% B for 10 min at a flow rate of 300 nL/min. Peptides were introduced to a TimsTOF HT (Bruker Daltonics) using a 20 µm ID fused silica emitter (Bruker Daltonics) installed in a nano-electrospray ion source (CaptiveSpray source, Bruker Daltonics) with spray voltage set to 1500 V.

For DIA acquisition, peptides were analyzed with a TimsTOF HT (Bruker Daltonics) running in DIA-PASEF mode. The DIA-PASEF method was optimized for the specific sample type using the py_diAID tool.[50] The method covered an ion mobility range from 1.35 to 0.7 Vs cm-*2* and an m/z range of 300 to 1300, using 10 DIA-PASEF scans with two isolation windows per scan, resulting in a cycle time of 1.1 s. Collision energy was linearly decreased from 59 eV at 1.6 Vs cm-*2* to 20 eV at 0.6 Vs cm-*2*. For all experiments the ion mobility dimension was calibrated linearly using three selected ions of the Agilent ESI LC/MS Tuning Mix [m/z, 1/K0: (322.0481, 0.7318 Vs cm−*2*), (622.0289, 0.9848 Vs cm−*2*), (922.0097, 1.1895 Vs cm−*2*)]. Mass calibration was performed with sodium formate in HPC mode.

Proteomics data analysis.

The raw files were analysed using DIA-NN (version 1.8.1). Searches were performed against a UniProt database of the mouse proteome (UPID: UP000000589, downloaded 17th March 2024).[51] The output file "report.unique_genes_matrix.tsv" from DIA-NN was used for further analysis in R Statistical Software.[52] At most 1 missing value in either the low- or high-uptake samples were allowed, and missing values were imputed with the average value of the remaining measurements. In cases where all values were missing from either the low- or high-uptake samples, the missing values were imputed with a negligible small number to allow for further processing and statistical calculations. Significantly differentially expressed proteins were determined using the empirical Bayes method in the Limma package[53] (Version 3.58.1) in R, and the significant proteins were determined to have a 2-fold difference between the expression levels of low- and high-uptake samples with an adjusted p-value of <0.05. Pathway analysis was performed using the clusterProfiler package in R.[54]

Fluorescence assay

cpFA stocks were diluted to 50 µM in a similar way to the uptake assay. In a black 96-well flat-bottom plate 100 µL of tetrazine-BODIPY FL (2 µM) was added to 100 µL of cpFA stock (50 µM) and left to react at room temperature for 1 hour. The plate was scanned for fluorescence on a CLARIOstar plate reader (BMG LABTECH) with excitation/emission at 477-14/530- 40 and dichroic filter 497 showing the turn-on ratio between the sample and negative control (1 µM BODIPY FL), as an average of the three samples.

Reagents and QC for cpFA synthesis

All commercially available reagents and solvents were used as received unless stated otherwise. Anhydrous solvents were prepared by storage over activated 3 Å (only for MeOH) or 4 Å molecular sieves. Reaction progress was determined via TLC (Sigma, TLC Silica gel 60 F254) via UV visualisation (λ = 254 nm) and potassium permanganate stain (6 g $KMnO_4$ and 40 g, K_2CO_3 in 600 mL water). All column chromatography purifications were performed using solvents as received and silica gel (Macherey-Nagel, Kieselgel 60 M, 0.04 – 0.63 mm). LC-MS analysis was performed on a Finnigan Surveyor HPLC system (detection at 200-600 nm) with an analytical C18 column (Gemini, 50 x 4.6 mm, 3 µm particle size, Phenomenex) coupled to a Finnigan LCQ Advantage MAX ion-trap mass spectrometer (ESI+). Solvent system: A: water (gradient, 50-90% or 10-90%), B: CH_3CN (gradient, 50-10% or 90-10%), C: (constant, 10%) 1% TFA (aq). High resolution mass spectrometry (HRMS) spectra were recorded by direct injection (2 µL of a 1 µM solution in $CH_3CN/H_2O/$*t*BuOH) on a Thermo Scientific Q Exactive HF Orbitrap mass spectrometer equipped with an electrospray ion source in positive-ion mode (source voltage 3.5 kV, sheath gas flow 10, capillary temperature 275 °C) with resolution R = 240,000 at m/z 400 (mass range m/z 160 – 2000) correlated to an external calibration (Thermo Finnigan). ^{1}H and ^{13}C NMR spectra were recorded using a Brüker AV-400 (400/101 MHz) or AV-500 (500/126 MHz). Chemical shift values are reported in ppm (δ) relative to the residual solvent signal of $CDCl_3$ (δ = 7.26 ppm for ^{1}H and δ = 77.16 ppm for ^{13}C NMR). Multiplicities are given as singlet (s), doublet (d), triplet (t), quartet (q), pentet (p), doublet of doublets (dd), broad singlet (br s) and multiplet (m). Recorded data was interpreted and analysed using MestReNova software.

References

1. Heieis, G. A., Patente, T. A., Almeida, L., Vrieling, F., Tak, T., Perona-Wright, G., Maizels, R. M., Stienstra, R. & Everts, B. Metabolic heterogeneity of tissue-resident macrophages in homeostasis and during helminth infection. *Nat. Commun.* **14**, 5627 (2023).
2. Makowski, L., Chaib, M. & Rathmell, J. C. Immunometabolism: From basic mechanisms to translation. *Immunol. Rev.* **295**, 5–14 (2020).
3. Kedia-Mehta, N. & Finlay, D. K. Competition for nutrients and its role in controlling immune responses. *Nat. Commun.* **10**, 2123 (2019).
4. Newsholme, P. Cellular and metabolic mechanisms of nutrient actions in immune function. *Eur. J. Clin. Nutr.* **75**, 1328–1331 (2021).
5. Bird, R. E., Lemmel, S. A., Yu, X. & Zhou, Q. A. Bioorthogonal Chemistry and Its Applications. *Bioconjug. Chem.* **32**, 2457–2479 (2021).
6. Scinto, S. L., Bilodeau, D. A., Hincapie, R., Lee, W., Nguyen, S. S., Xu, M., Am Ende, C. W., Finn, M. G., Lang, K., Lin, Q., Pezacki, J. P., Prescher, J. A., Robillard, M. S. & Fox, J. M. Bioorthogonal chemistry. *Nat. Rev. Methods Primer* **1**, 30 (2021).
7. Best, M. D. Click chemistry and bioorthogonal reactions: unprecedented selectivity in the labeling of biological molecules. *Biochemistry* **48**, 6571–6584 (2009).

8. Rigolot, V., Biot, C. & Lion, C. To View Your Biomolecule, Click inside the Cell. *Angew. Chem. Int. Ed Engl.* **60**, 23084–23105 (2021).
9. Pelgrom, L. R., Davis, G. M., O'Shaughnessy, S., Wezenberg, E. J. M., Van Kasteren, S. I., Finlay, D. K. & Sinclair, L. V. QUAS-R: An SLC1A5-mediated glutamine uptake assay with single-cell resolution reveals metabolic heterogeneity with immune populations. *Cell Rep.* **42**, 112828 (2023).
10. Kuerschner, L., Leyendecker, P., Klizaite, K., Fiedler, M., Saam, J. & Thiele, C. Development of oxaalkyne and alkyne fatty acids as novel tracers to study fatty acid beta-oxidation pathways and intermediates. *J. Lipid Res.* **63**, 100188 (2022).
11. Hang, H. C., Wilson, J. P. & Charron, G. Bioorthogonal chemical reporters for analyzing protein lipidation and lipid trafficking. *Acc. Chem. Res.* **44**, 699–708 (2011).
12. Beavers, W. N., Serwa, R., Shimozu, Y., Tallman, K. A., Vaught, M., Dalvie, E. D., Marnett, L. J. & Porter, N. A. ω-Alkynyl lipid surrogates for polyunsaturated fatty acids: free radical and enzymatic oxidations. *J. Am. Chem. Soc.* **136**, 11529–11539 (2014).
13. Bertheussen, K., van de Plassche, M., Bakkum, T., Gagestein, B., Ttofi, I., Sarris, A. J. C., Overkleeft, H. S., van der Stelt, M. & van Kasteren, S. I. Live-Cell Imaging of Sterculic Acid-a Naturally Occurring 1,2-Cyclopropene Fatty Acid-by Bioorthogonal Reaction with Turn-On Tetrazine-Fluorophore Conjugates. *Angew. Chem. Int. Ed Engl.* **61**, e202207640 (2022).
14. Blackman, M. L., Royzen, M. & Fox, J. M. Tetrazine ligation: fast bioconjugation based on inverse-electron-demand Diels-Alder reactivity. *J. Am. Chem. Soc.* **130**, 13518–13519 (2008).
15. Devaraj, N. K., Upadhyay, R., Haun, J. B., Hilderbrand, S. A. & Weissleder, R. Fast and sensitive pretargeted labeling of cancer cells through a tetrazine/trans-cyclooctene cycloaddition. *Angew. Chem. Int. Ed Engl.* **48**, 7013–7016 (2009).
16. Oliveira, B. L., Guo, Z. & Bernardes, G. J. L. Inverse electron demand Diels-Alder reactions in chemical biology. *Chem. Soc. Rev.* **46**, 4895–4950 (2017).
17. Eisenbarth, S. C. Dendritic cell subsets in T cell programming: location dictates function. *Nat. Rev. Immunol.* **19**, 89–103 (2019).
18. Wolf, T., Jin, W., Zoppi, G., Vogel, I. A., Akhmedov, M., Bleck, C. K. E., Beltraminelli, T., Rieckmann, J. C., Ramirez, N. J., Benevento, M., Notarbartolo, S., Bumann, D., Meissner, F., Grimbacher, B., Mann, M., Lanzavecchia, A., Sallusto, F., Kwee, I. & Geiger, R. Dynamics in protein translation sustaining T cell preparedness. *Nat. Immunol.* **21**, 927–937 (2020).
19. Michalek, R. D., Gerriets, V. A., Jacobs, S. R., Macintyre, A. N., MacIver, N. J., Mason, E. F., Sullivan, S. A., Nichols, A. G. & Rathmell, J. C. Cutting edge: distinct glycolytic and lipid oxidative metabolic programs are essential for effector and regulatory CD4+ T cell subsets. *J. Immunol. Baltim. Md 1950* **186**, 3299–3303 (2011).
20. Berod, L., Friedrich, C., Nandan, A., Freitag, J., Hagemann, S., Harmrolfs, K., Sandouk, A., Hesse, C., Castro, C. N., Bähre, H., Tschirner, S. K., Gorinski, N., Gohmert, M., Mayer, C. T., Huehn, J., Ponimaskin, E., Abraham, W.-R., Müller, R., Lochner, M. & Sparwasser, T. De novo fatty acid synthesis controls the fate between regulatory T and T helper 17 cells. *Nat. Med.* **20**, 1327–1333 (2014).
21. Thurnher, M. & Gruenbacher, G. T lymphocyte regulation by mevalonate metabolism. *Sci. Signal.* **8**, re4–re4 (2015).
22. Abdelmagid, S. A., Clarke, S. E., Nielsen, D. E., Badawi, A., El-Sohemy, A., Mutch, D. M. & Ma, D. W. L. Comprehensive Profiling of Plasma Fatty Acid Concentrations in Young Healthy Canadian Adults. *PLoS ONE* **10**, e0116195 (2015).
23. Adams, J. & Spero, D. M. Rhodium (II) catalyzed reactions of diazo-carbonyl compounds. *Tetrahedron* **47**, 1765–1808 (1991).
24. Maryanoff, B. E. & Reitz, A. B. The Wittig olefination reaction and modifications involving phosphoryl-stabilized carbanions. Stereochemistry, mechanism, and selected synthetic aspects. *Chem. Rev.* **89**, 863–927 (1989).

25. Oger, C., Balas, L., Durand, T. & Galano, J.-M. Are alkyne reductions chemo-, regio-, and stereoselective enough to provide pure (Z)-olefins in polyfunctionalized bioactive molecules? *Chem. Rev.* **113**, 1313–1350 (2013).
26. Lin, L., Hu, M., Li, Q., Du, L., Lin, L., Xue, Y., Zheng, F., Wang, F., Liu, K., Wang, Y., Ye, J., Jiang, X., Wang, X., Wang, J., Zhai, J., Liu, B., Xie, H., You, Y., Wang, J., Kong, X., Feng, D., Green, D. R., Shi, Y. & Wang, Y. Oleic acid availability impacts thymocyte preprogramming and subsequent peripheral Treg cell differentiation. *Nat. Immunol.* **25**, 54–65 (2024).
27. Ivanov, I. I., de Llanos Frutos, R., Manel, N., Yoshinaga, K., Rifkin, D. B., Sartor, R. B., Finlay, B. B. & Littman, D. R. Specific microbiota direct the differentiation of Th17 cells in the mucosa of the small intestine. *Cell Host Microbe* **4**, 337–349 (2008).
28. Basu, R., O'Quinn, D. B., Silberger, D. J., Schoeb, T. R., Fouser, L., Ouyang, W., Hatton, R. D. & Weaver, C. T. Th22 Cells are an Important Source of IL-22 for Host Protection against Enteropathogenic Bacteria. *Immunity* **37**, 1061–1075 (2012).
29. Sinclair, L. V., Barthelemy, C. & Cantrell, D. A. Single Cell Glucose Uptake Assays: A Cautionary Tale. *Immunometabolism* **2**, e200029 (2020).
30. Samovski, D., Jacome-Sosa, M. & Abumrad, N. A. Fatty Acid Transport and Signaling: Mechanisms and Physiological Implications. *Annu. Rev. Physiol.* **85**, 317–337 (2023).
31. Schwenk, R. W., Holloway, G. P., Luiken, J. J. F. P., Bonen, A. & Glatz, J. F. C. Fatty acid transport across the cell membrane: Regulation by fatty acid transporters. *Prostaglandins Leukot. Essent. Fat. Acids PLEFA* **82**, 149–154 (2010).
32. Neef, A. B. & Schultz, C. Selective fluorescence labeling of lipids in living cells. *Angew. Chem. Int. Ed Engl.* **48**, 1498–1500 (2009).
33. Kuerschner, L. & Thiele, C. Tracing Lipid Metabolism by Alkyne Lipids and Mass Spectrometry: The State of the Art. *Front. Mol. Biosci.* **9**, (2022).
34. Hein, J. E. & Fokin, V. V. Copper-catalyzed azide–alkyne cycloaddition (CuAAC) and beyond: new reactivity of copper(i) acetylides. *Chem. Soc. Rev.* **39**, 1302–1315 (2010).
35. Fantoni, N. Z., El-Sagheer, A. H. & Brown, T. A Hitchhiker's Guide to Click-Chemistry with Nucleic Acids. *Chem. Rev.* **121**, 7122–7154 (2021).
36. Lawless, S. J., Kedia-Mehta, N., Walls, J. F., McGarrigle, R., Convery, O., Sinclair, L. V., Navarro, M. N., Murray, J. & Finlay, D. K. Glucose represses dendritic cell-induced T cell responses. *Nat. Commun.* **8**, 15620 (2017).
37. Chang, C.-H., Qiu, J., O'Sullivan, D., Buck, M. D., Noguchi, T., Curtis, J. D., Chen, Q., Gindin, M., Gubin, M. M., van der Windt, G. J. W., Tonc, E., Schreiber, R. D., Pearce, E. J. & Pearce, E. L. Metabolic Competition in the Tumor Microenvironment Is a Driver of Cancer Progression. *Cell* **162**, 1229–1241 (2015).
38. Reinfeld, B. I. *et al.* Cell-programmed nutrient partitioning in the tumour microenvironment. *Nature* **593**, 282–288 (2021).
39. Guo, C., You, Z., Shi, H., Sun, Y., Du, X., Palacios, G., Guy, C., Yuan, S., Chapman, N. M., Lim, S. A., Sun, X., Saravia, J., Rankin, S., Dhungana, Y. & Chi, H. SLC38A2 and glutamine signalling in cDC1s dictate anti-tumour immunity. *Nature* **620**, 200–208 (2023).
40. Angela, M., Endo, Y., Asou, H. K., Yamamoto, T., Tumes, D. J., Tokuyama, H., Yokote, K. & Nakayama, T. Fatty acid metabolic reprogramming via mTOR-mediated inductions of PPARγ directs early activation of T cells. *Nat. Commun.* **7**, 13683 (2016).
41. Nava Lauson, C. B., Tiberti, S., Corsetto, P. A., Conte, F., Tyagi, P., Machwirth, M., Ebert, S., Loffreda, A., Scheller, L., Sheta, D., Mokhtari, Z., Peters, T., Raman, A. T., Greco, F., Rizzo, A. M., Beilhack, A., Signore, G., Tumino, N., Vacca, P., McDonnell, L. A., Raimondi, A., Greenberg, P. D., Huppa, J. B., Cardaci, S., Caruana, I., Rodighiero, S., Nezi, L. & Manzo, T. Linoleic acid potentiates CD8+ T cell metabolic fitness and antitumor immunity. *Cell Metab.* **35**, 633-650.e9 (2023).
42. Lavin, Y., Winter, D., Blecher-Gonen, R., David, E., Keren-Shaul, H., Merad, M., Jung, S. & Amit, I. Tissue-resident macrophage enhancer landscapes are shaped by the local microenvironment. *Cell* **159**, 1312–1326 (2014).

43. Frizzell, H., Fonseca, R., Christo, S. N., Evrard, M., Cruz-Gomez, S., Zanluqui, N. G., von Scheidt, B., Freestone, D., Park, S. L., McWilliam, H. E. G., Villadangos, J. A., Carbone, F. R. & Mackay, L. K. Organ-specific isoform selection of fatty acid-binding proteins in tissue-resident lymphocytes. *Sci. Immunol.* **5**, eaay9283 (2020).
44. Reina-Campos, M., Heeg, M., Kennewick, K., Mathews, I. T., Galletti, G., Luna, V., Nguyen, Q., Huang, H., Milner, J. J., Hu, K. H., Vichaidit, A., Santillano, N., Boland, B. S., Chang, J. T., Jain, M., Sharma, S., Krummel, M. F., Chi, H., Bensinger, S. J. & Goldrath, A. W. Metabolic programs of T cell tissue residency empower tumour immunity. *Nature* **621**, 179–187 (2023).
45. Yan, J., Zeng, Y., Guan, Z., Li, Z., Luo, S., Niu, J., Zhao, J., Gong, H., Huang, T., Li, Z., Deng, A., Wen, Q., Tan, J., Jiang, J., Bao, X., Li, S., Sun, G., Zhang, M., Zhi, M., Yin, Z., Sun, W.-Y., Li, Y.-F., He, R.-R. & Cao, G. Inherent preference for polyunsaturated fatty acids instigates ferroptosis of Treg cells that aggravates high-fat-diet-related colitis. *Cell Rep.* **43**, (2024).
46. Dhar, S., Sarkar, T., Bose, S., Pati, S., Chakraborty, D., Roy, D., Panda, A. K., Guin, A., Mukherjee, S., Jana, K., Sarkar, D. K. & Sa, G. FOXP3 Transcriptionally Activates Fatty Acid Scavenger Receptor CD36 in Tumour-Induced Treg Cells. *Immunology* **174**, 296–309 (2025).
47. Wang, H., Franco, F., Tsui, Y.-C., Xie, X., Trefny, M. P., Zappasodi, R., Mohmood, S. R., Fernández-García, J., Tsai, C.-H., Schulze, I., Picard, F., Meylan, E., Silverstein, R., Goldberg, I., Fendt, S.-M., Wolchok, J. D., Merghoub, T., Jandus, C., Zippelius, A. & Ho, P.-C. CD36-mediated metabolic adaptation supports regulatory T cell survival and function in tumors. *Nat. Immunol.* **21**, 298–308 (2020).
48. Couturier, J., Nuotio-Antar ,Alli M., Agarwal ,Neeti, Wilkerson ,Gregory K., Saha ,Pradip, Kulkarni ,Viraj, Lakhashe ,Samir K., Esquivel ,Juan, Nehete ,Pramod N., Ruprecht ,Ruth M., Sastry ,K. Jagannadha, Meyer ,Jennifer M., Hill ,Lori R., Lake ,Jordan E., Balasubramanyam ,Ashok & and Lewis, D. E. Lymphocytes upregulate CD36 in adipose tissue and liver. *Adipocyte* **8**, 154–163 (2019).
49. Calder, P. C. The relationship between the fatty acid composition of immune cells and their function. *Prostaglandins Leukot. Essent. Fatty Acids* **79**, 101–108 (2008).

Figures

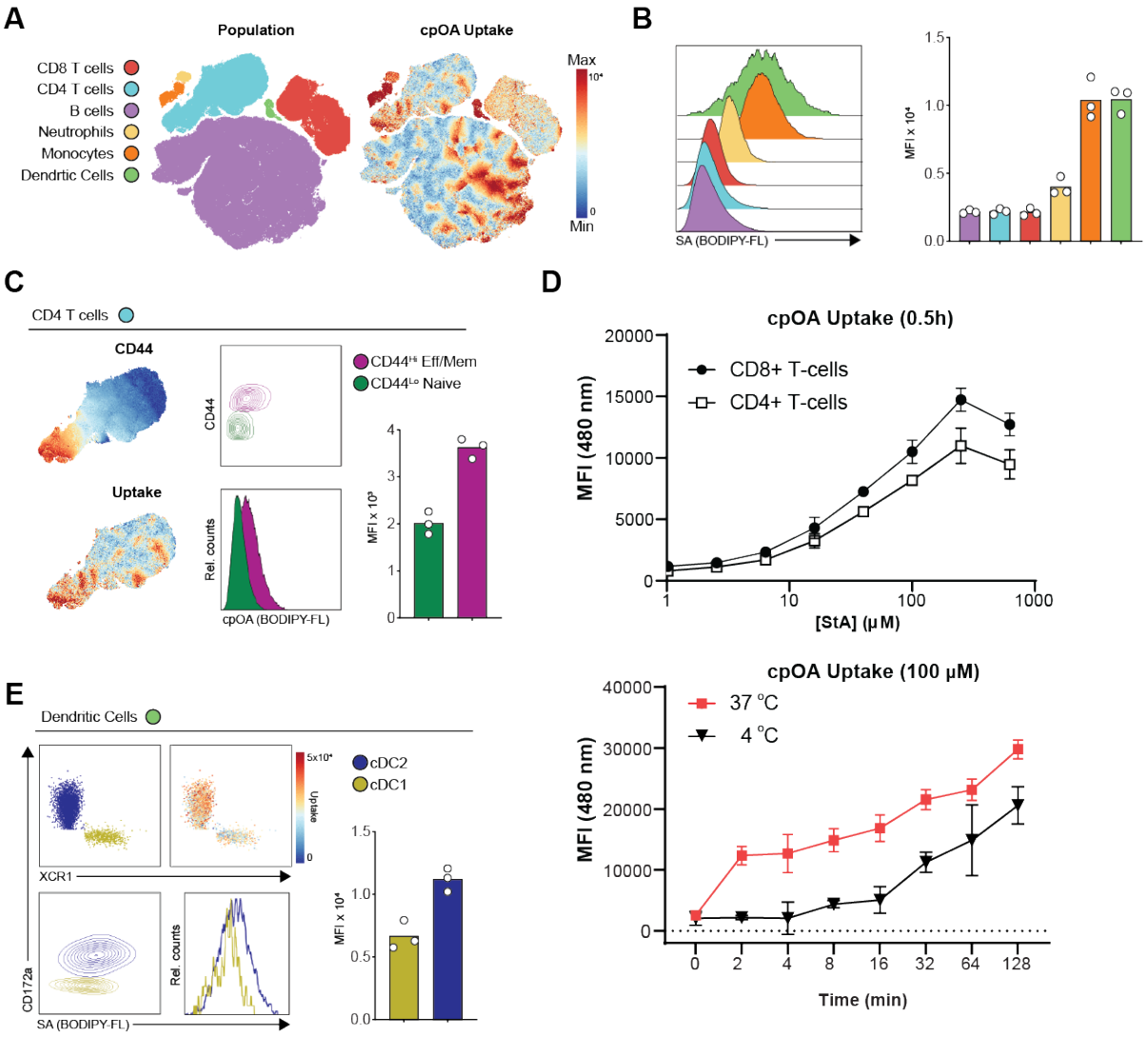

Figure 1: primary immune cell uptake of a cycolpropene modified oleic acid. A) Overlay of manually gated immune populations from the spleen, and relative cpOA uptake on a unifold mapping approximation and projection (UMAP) of immune cell markers. B) Representative histograms and quantification of the median fluorescent intensity (MFI) for cpOA uptake in splenocytes. C) Relative cpFA uptake and CD44 expression overlaid on the CD4+ T cells population isolated from (A), and representative histogram, contour plots and quantification of cpOA uptake. D) cpOA uptake by in vitro activated CD4/8 T cells (baseline is unactivated control) at different concentrations (top) and over time at 37 and 4 degrees. E) Representative plots and quantification of cpOA uptake in gated DC1 and DC2 populations. Data shown are means and data points for individual mice, N=3. Representative of one experiment.

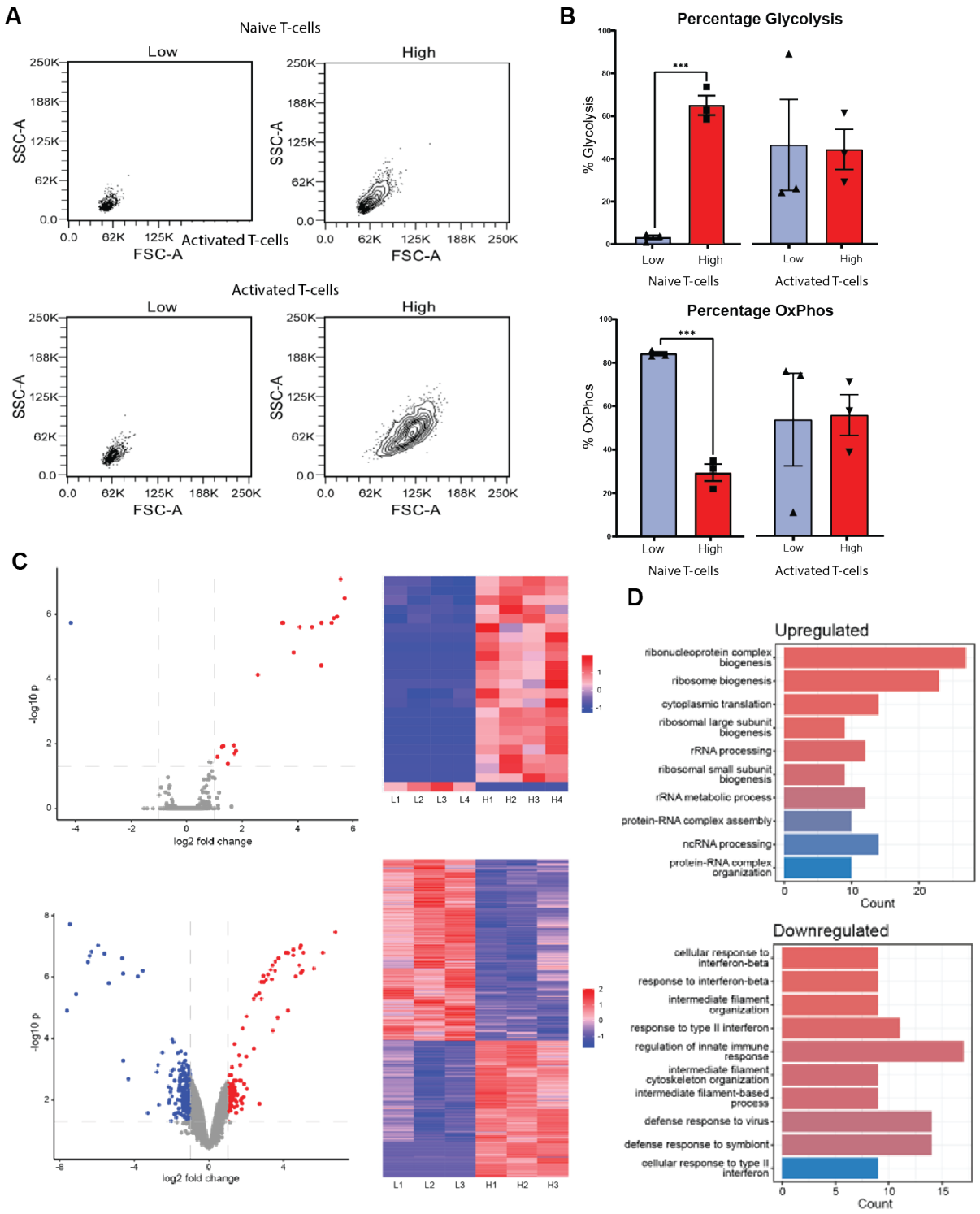

Figure 2: Live cell-sorting according to cpFA for downstream omics analyses. A) forward and side scatter analysis of low/high uptake subpopulations of naïve (top) and activated (bottom) CD3/CD4+ T cells. B) Metabolic flux analysis of activated and naïve T cells. Glycolysis (top) and oxphos (bottom) vary between low/high naïve subpopulations of T cells but not between the subpopulations of activated T cells. C) volcanoplots of proteomics performed on high/low cpOA uptake naïve and activated T cells. Heatmaps show the differences in up/downregulation between biological replicates (N=4 and N=3 respectively) D) pathway analysis of up/downregulated pathways of activated T cells.

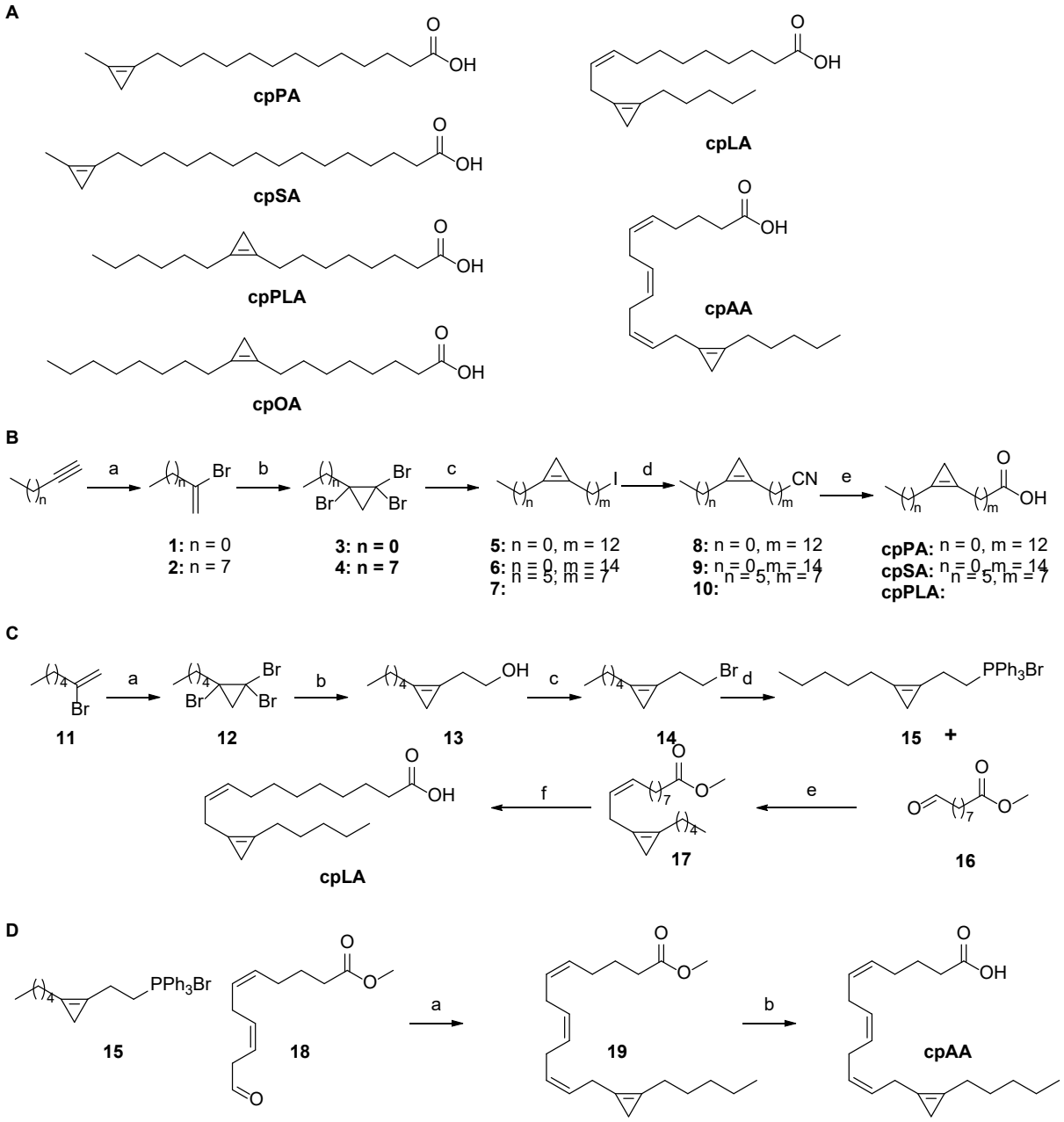

Figure 3. Synthesis of cyclopropene FA analogue synthesis. A) Library of synthesized cp-containing FA analogues. B) Synthesis of cpFAs containing no additional double bonds. Reagents and conditions: a) BBr_3, DCM, -78 °C to rt, 3 h, 78% yield. b) NaOH, CTAB, $CHBr_3$, DCM, 0 °C to rt, 18 h, 47% – 57% yield. c) *n*-BuLi, diiodoalkane, THF, -78 °C to 0 °C, 4 h, 27 – 56% yield. d) NaCN, DMSO, 90 °C, 1 h, 68 – 89% yield. e) NaOH, EtOH / water, reflux, 18 h, 37 – 63% yield. C) Synthesis of cpLA. Reagents and conditions: a) BBr_3, DCM, -78 °C to rt, 3 h, 52% yield. b) *n*-Buli, $BF_3{\cdot}OEt_2$, oxirane, THF, -78 °C to 0 °C, 2 h, 49% yield. c) NBS, PPh_3, DCM, 0 °C to rt, 2 h, 59% yield. d) PPh_3, MeCN, 82 °C, 18 h, 82% yield. e) NaHMDS, THF, -78 °C to 0 °C, 2.5 h, 44% yield. f) NaOH (aq.), 1:1 THF / EtOH, 70 °C, 2 h, 73% yield. D) Synthetic route towards cpAA. Reagents and conditions: a) NaHMDS, THF, -78 °C to 0 °C, 2.5 h, 54% yield. b) NaOH (aq.), 1:1 THF / EtOH, 70 °C, 2 h, quant. yield.

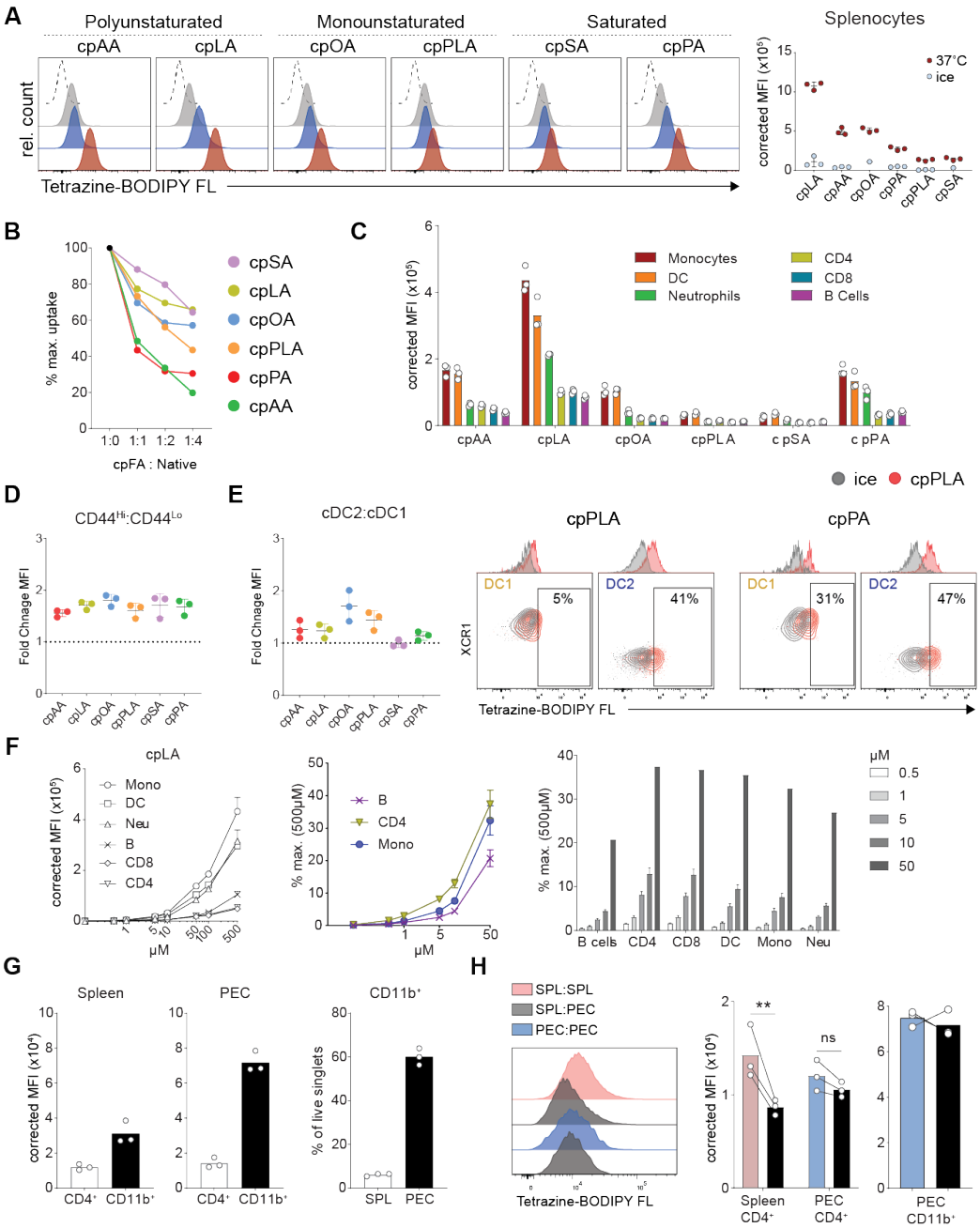

Figure 4: Uptake and competition of novel cpFA by primary splenocytes. A)Representative histograms for cpFA uptake in primary splenocytes, and corresponding controls with either no click reaction performed (no click), click reaction performed without the cpFA pulse (no cpFA), cpFA pulsed on ice or at 37°C prior to performing the click reaction. B) Relative decrease in cpFA uptake when pulsed with increasing concentrations of the corresponding native species, calculated as percent MFI of uncompleted cpFA. C) Background subtracted MFI of indicated cpFA species for major immune lineages within the murine spleen. D) Ratio of cpFA MFI for CD44hi effector/memory relative to CD44lo naïve CD4+ T cells. E) Ratio of cpFA MFI for CD172a+ DC2 relative to XCR1+ DC1 and representative contour plots for polyunsaturated cpPLA and saturated cpPA with frequency of positive cells compared to ice controls. F) Titration of increasing cpLA concentrations in splenocyte populations as indicated showing background corrected MFI and % uptake from the highest concentration tested. G) Uptake of CD4+ T cell and CD11b+ myeloid populations, and their frequency of total immune cells within the tissue, for the spleen and peritoneal cell exudate (PEC). H) Total splenocytes or PEC were cultured individually or at a 1:1 mixed ratio after CD45-labelling. Representative histograms and pair-

wise comparison of cpLA uptake in CD4+ T cells or CD11b+ myeloid cells from individual or mixed cultures. Data represent mean and SD of individual mice. Representative of one (B,D,E,G,H) or two (A,C,F) experiments. Statistics done using two-way repeated measures ANOVA, ** $p < 0.01$, ns = not significant.

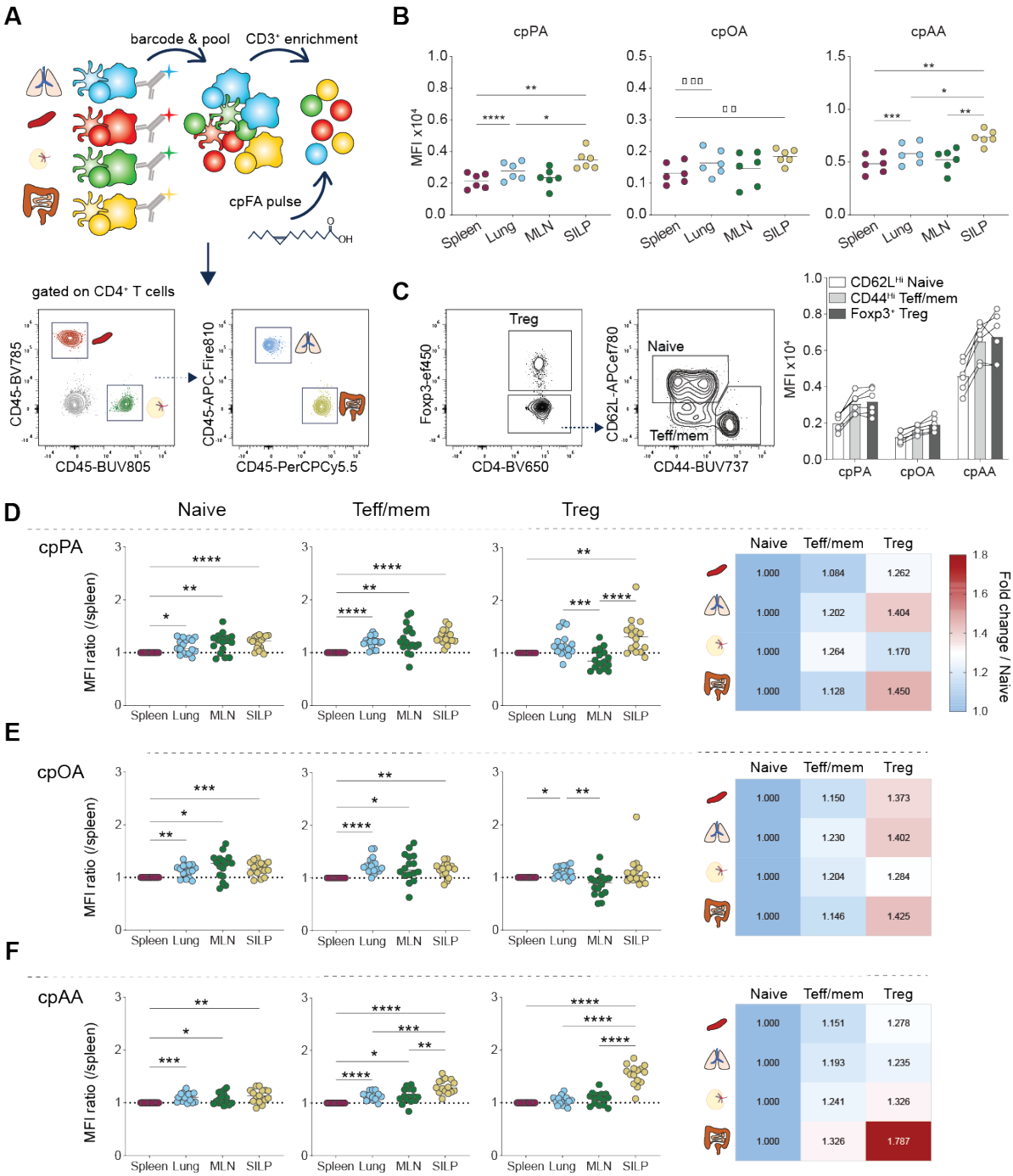

Figure 5: Distinct cpFA uptake patterns in regulatory T cells across tissues. A) Experimental barcoding scheme to determine cell-intrinsic differences in T cell cpFA uptake. B) Background corrected MFI for total CD4+ T cell uptake of indicated cpFA across tissues. C) Representative gating of CD4+ T cell populations in the spleen and background corrected MFI indicating cpFA uptake between Naïve, Teff/mem and Tregs. D) Graphs showing MFI of population from each tissue normalized to the spleen, and heatmap showing the median fold change of MFI normalized to naïve T cells for each individual tissue, for saturated cpPA, E) monounsaturated cpOA, F) polyunsaturated cpAA. CD4 T cell uptake of

cpOA and cpAA measured after one or three days of in vitro activation or polarization towards Tregs. Quantified background corrected MFI, representative histograms and relative increased from day one to day three shown. Data points representative individual mice and mean representative for pooled from three independent experiments with n=3-7 mice (B-F), or technical replicates from of one experiments. Statistics determined by repeated measures one-way ANOVA or two-tailed t-test. **** p < 0.0001, *** p < 0.001, ** p < 0.01, * p < 0.05, ns = not significant.

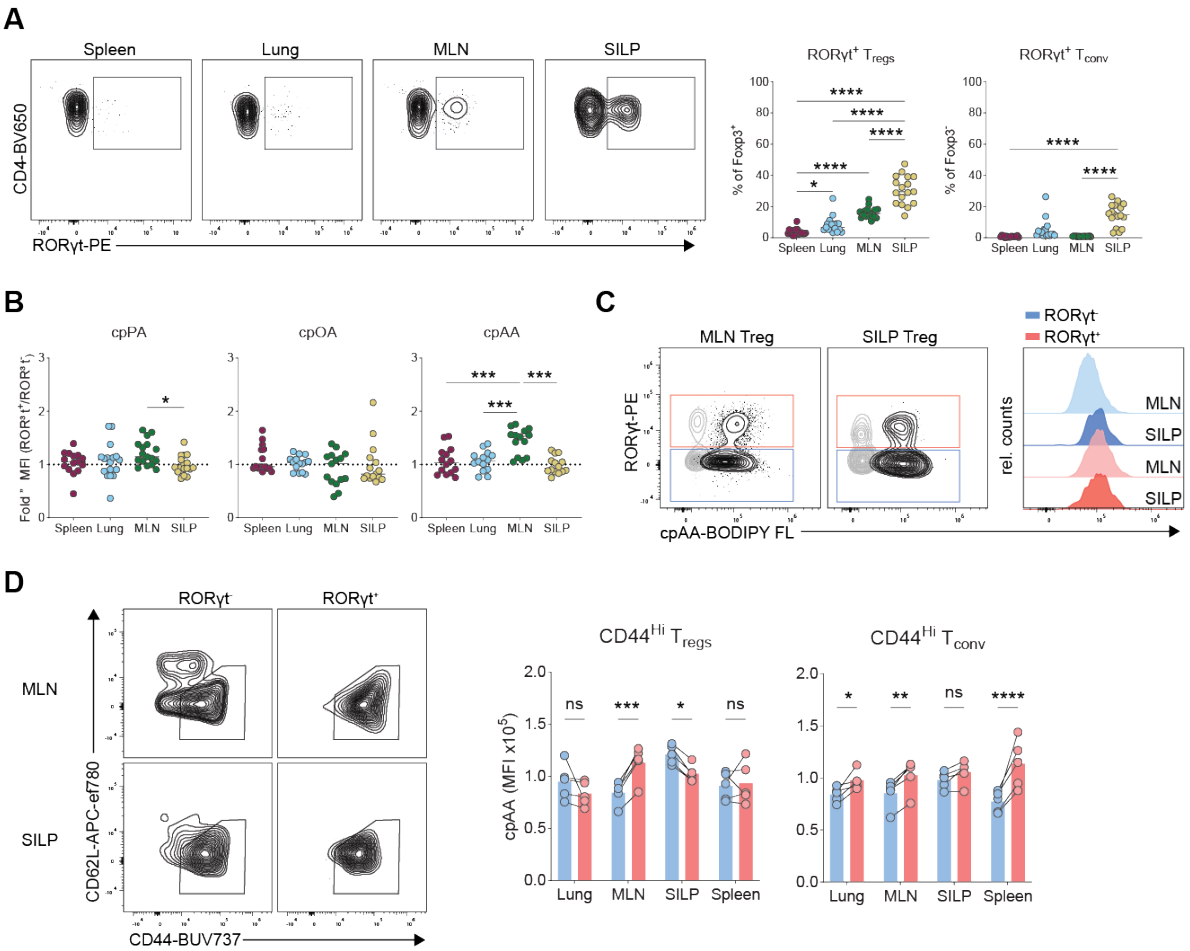

Figure 6: Evidence of cell-intrinsic and environmental drivers of cpAA uptake in tissue Tregs. A) Representative gating of RORγt+ Tregs, and frequencies of RORgt+ Tregs or RORgt+ Foxp3- conventional CD4+ T cells. B) Ratio of cpFA uptake between RORgt+ and RORgt- Foxp3+ Tregs. C) Contour plots and histograms of RORgt+ and RORgt- Treg cpAA uptake from the MLN and SILP concatenated from six mice. D) Gating of CD44HiCD62L Tregs within RORgt subsets from the MLN and SILP and comparison of background subtracted MFI between CD44Hi RORgt+ and CD44Hi RORgt- cells within each tissue. Data show means and datapoints for individual mice either pooled or shown as one representative of three independent experiments with 3-7 mice per experiment. Comparison done using one or two-way ANOVA with repeated measures. **** p < 0.0001, *** p < 0.001, ** p < 0.01, * p < 0.05, ns = not significant.